Optical Materials 66 (2017) 480–486

Contents lists available at ScienceDirect

Optical Materials

journal homepage: www.elsevier.com/locate/optmat

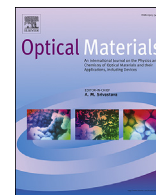

Analysis of electrical properties of heterojunction based on $ZnIn_2Se_4$

A.A. Attia [a], H.A.M. Ali [a, *], G.F. Salem [a], M.I. Ismail [a], F.F. Al-Harbi [b]

[a] Physics Department, Faculty of Education, Ain Shams University, Roxy, 11757, Cairo, Egypt
[b] Department of Physics, College of Science, Princess Nora Bint Abdulrahman University, Riyadh, Saudi Arabia

A R T I C L E I N F O

Article history:
Received 18 January 2017
Received in revised form
22 February 2017
Accepted 26 February 2017

Keywords:
Heterojunction
Transport mechanisms
Junction parameters
Photovoltaic characteristics

A B S T R A C T

Heterojunction of n-$ZnIn_2Se_4$/p-Si was fabricated using thermal evaporation of $ZnIn_2Se_4$ thin films of thickness 473 nm onto p-Si substrate at room temperature. The characteristics of current–voltage (I-V) for n-$ZnIn_2Se_4$/p-Si heterojunction were investigated at different temperatures ranged from 308 K to 363 K. The junction parameters namely are; rectification ratio (RR), series resistance (R_s), shunt resistance (R_{sh}) and diode ideality factor (n) were calculated from the analysis of I-V curves. The forward current showed two conduction mechanisms operating, which were the thermionic emission and the single trap space charge limited current in low ($0 \leq V \leq 0.5$ **V**) and high ($V \geq 0.7$ **V**) ranges of voltage, respectively. The reverse current was due to the generation through Si rather than the $ZnIn_2Se_4$ film. The built-in voltage and the width of the depletion region were determined from the capacitance-voltage (C-V) measurements. The photovoltaic characteristics of the junction were also studied through the (I-V) measurements under illumination of 40 mW/cm^2. The cell parameters; the short-circuit current, the open-circuit voltage and the fill factor were estimated at room temperature.

© 2017 Elsevier B.V. All rights reserved.

1. Introduction

The heterojunctions based on a combination of amorphous and crystalline semiconductors attract an attention [1] due to their great potential in numerous applications [2–5]. There is an interest for chalcogenide films that are related to device applications and formation of interfaces of chalcogenide semiconductors with the crystalline semiconductors such as germanium, silicon and III-V compounds. Altering chalcogenide glasses lead to change the electronic properties of the interfaces [6]. These semiconductors are widely used in solid-state such as infrared detector, photovoltaic cells, nuclear radiation detector and windows for infrared laser [7]. Ternary chalcogenides belonging to the AB_2X_4 (A:Zn,Cd,Hg,B:Al,Ga,In,X:S,Se,Te) are class of semiconductors that cover many areas of fundamental and technological interest [8]. These compounds are defect chalcopyrites [9]. The crystal lattices of these systems are characterized by a vacancy sublattice and a distorted cationic sublattice, which can be occupied by metal atoms A and B with a different degree of order that creates different structural models. Thus, different types of the same compound can be isolated [10]. The suitable elements that can occupy the vacancies at the cation lead to modify the physical properties of these compounds [9]. The phonon anharmonicity is a substantial in these compounds. A physical effect that requires phonon anharmonicity as a key ingredient is thermal conductivity. Hence, the scattering of phonons from lattice defects would produce a finite thermal conductivity. Also, the increased anharmonicity will enhance the phonon-phonon scattering and thus reduces the thermal conductivity [11].

$ZnIn_2Se_4$ semiconducting compound attracts the attention of many researchers due to its potential application in various fields, including photo-electronic, photo-voltaic and switching memory devices [12–15]. The defect in $ZnIn_2Se_4$ arises from some percentage vacancies of Zn sites and naturally disorder is produced that causes the appearance of a large number of electronic levels in the energy gap [16]. Every Se atom is tetrahedrally surrounded by a vacancy and three cationic sites occupied by the metal atoms with ratio 2/3 of In and 1/3 of Zn. The existence of a vacant site in the tetrahedral coordination of the Se atom lets the anion to displace far from the metal ions towards the vacancy [17]. Some studies on structural and electronic properties of chalcopyrite semiconductors are carried out using some methods depending on the density functional theory (DFT), and compared its results with those obtained experimentally [18–20].

In the present work, a heterojunction of Au/n-$ZnIn_2Se_4$/p-Si/Al was fabricated by thermal evaporation technique. The

* Corresponding author.
E-mail address: hend2061@yahoo.com (H.A.M. Ali).

http://dx.doi.org/10.1016/j.optmat.2017.02.055
0925-3467/© 2017 Elsevier B.V. All rights reserved.

characteristics of current –voltage (I-V) measurements of the heterojunction were studied in the dark condition at different temperatures; ranged from 308 K to 363 K. The junction parameters and the current transport mechanisms were deduced. The capacitance – voltage (C-V) measurements were indexed at room temperature to determine the built-in voltage and the width of depletion region besides the type of the heterojunction. The photovoltaic properties were also investigated to obtain the solar cell parameters of n-$ZnIn_2Se_4$/p-Si heterojunction.

2. Experimental techniques

$ZnIn_2Se_4$ Ingot was prepared by fusion of stoichiometric quantities of pure elements in evacuated sealed silica tubes, which were left at 1323 K for 10 h. Then, the ingot cooled to room temperature over 48 h. Thin films of $ZnIn_2Se_4$ were deposited onto etched Silicon wafer (p-type) as substrates to fabricate n-$ZnIn_2Se_4$/p-Si heterojunction. The deposition was carried out by the thermal evaporation technique using the vacuum coating unite (Edwards, E306A), under a vacuum of about 10^{-4} Pa. The deposition was made at room temperature with a rate of 2 nm/s. The deposition rate and $ZnIn_2Se_4$ film thickness were controlled utilizing quartz thickness monitor (model FTM4 Edwards). In the fabrication of the heterojunction, a polished p-Si crystal wafer with (100) orientation parallel to the surface, holes concentration of 10^{16} cm^{-3} and thickness of 250 μm was used. The p-Si wafer was chemically cleaned and etched by a solution ($HF:HNO_3:CH_3COOH$ in ratio 1:6:1) for 10 s. Then, it rinsed with deionized water and isopropyl alcohol and oven-dried. The bottom electrode was made by evaporating Aluminum (Al) onto backside of Si. On the another side of Si, a $ZnIn_2Se_4$ film of thickness 473 nm was deposited. The top gold (Au) electrode was then deposited in the form of mesh onto the $ZnIn_2Se_4$ film. The configuration of the resultant Au/n-$ZnIn_2Se_4$/p-Si/Al heterojunction was depicted in Fig. 1. The measurements of current–voltage were carried out using a high impedance programmable electrometer (Keithley 2635A). The measurements were carried out in a dark condition at temperature range 308–363 K. The temperature of the heterojunction was measured using a Chromel-Alumel thermocouple connected to a digital thermometer. The capacitance-voltage measurements of Au/n-$ZnIn_2Se_4$/p-Si/Al heterojunction were made at 1 MHz using a computerized CV-410 meter (Solid State Measurement, Inc., Pittsburgh) at room temperature. The photovoltaic measurements of the cell were carried out under the illumination of white light of a tungsten lamp with intensity of 40 mW/cm^2 at room temperature. The distance between the cell and the tungsten lamp was 20 cm.

3. Results and discussion

Structural studies using X-ray diffraction are carried out for the prepared $ZnIn_2Se_4$ in the powder and thin films forms in our previous work [21]. The results revealed that the powder of $ZnIn_2Se_4$ has a polycrystalline nature of tetragonal structure with lattice parameters a = 5.5952 Å and c = 11.9886 Å.

The electrical properties of n-$ZnIn_2Se_4$/p-Si are investigated at different temperatures; ranged from 308 K to 363 K. Fig. 2a represents I-V characteristics of n-$ZnIn_2Se_4$/p-Si heterojunction under the applied voltage of range (−2 to 2 V) at different temperatures. It is seen that the current increases with increasing voltage in the forward and reverse bias conditions at different temperatures. The I–V curves showed asymmetrical and non-linear behavior as observed by Yadav et al. [22]. Thus the $ZnIn_2Se_4$/Si heterojunction exhibits diode-like behavior due to the formation of a depletion region between $ZnIn_2Se_4$ and Si that limits the forward and reverse carrier flowing across the junction [23]. The values of current in the forward bias region is found to be higher than those of the reverse one as seen in Fig. 2b. This indicates a rectifying nature of the n-$ZnIn_2Se_4$/p-Si heterojunction [24]. The rectification ratio (RR) of the heterojunction is the ratio of the forward to the reverse currents at certain constant applied voltage. For the investigated n-$ZnIn_2Se_4$/p-Si heterojunction, RR is calculated at ± 1 **V** and it was found to be 26.74. The values of RR at different temperatures were calculated and listed in Table 1. It was seen that the rectification ratio decreases with increasing temperature. This behavior can be due to the increase in leakage current with increasing temperature [25].

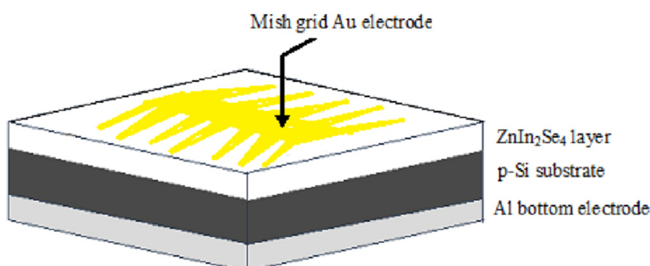

Fig. 1. The configuration for the structure of n-$ZnIn_2Se_4$/p-Si heterojunction.

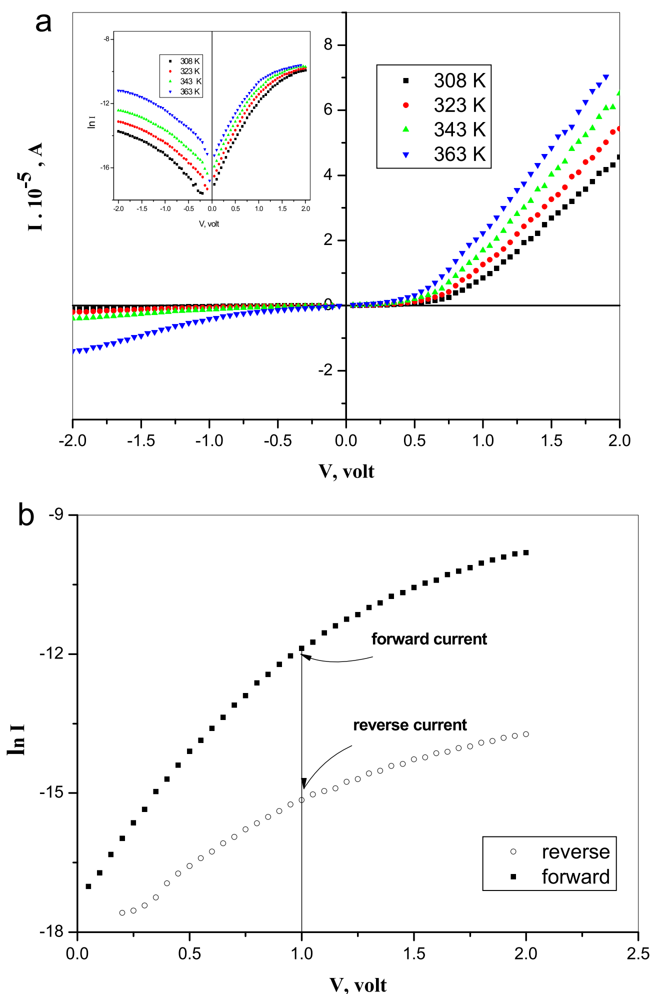

Fig. 2. a): I-V characteristics of n-$ZnIn_2Se_4$/p-Si heterojunction at different temperature and the voltage dependence of lnI inset it. b): Semilogarithmic plot of the forward and reserve current of n-$ZnIn_2Se_4$/p-Si heterojunction against voltage at room temperature.

Table 1
The estimated values of RR, R_s, R_{sh} and *n* for n-$ZnIn_2Se_4$/p-Si heterojunction at different temperatures.

T (K)	RR	R_s (kΩ)	R_{sh} (MΩ)	*n*
308	26.74	20	31.6	5.6
323	23.35	14.2	4.2	5.47
343	14.58	12	2.3	5.28
363	5.38	11	0.62	5.34
[22]	–	0.165	0.018	5.6
303 [33]	345.5 × 10^3	0.30	0.146	1.281

The forward current of a p-n junction is given by the following equation [26]:

$$I = I_o\left[e^{\left(\frac{q(V-IR_S)}{nkT}\right)} - 1\right] + \frac{V - IR_S}{R_{sh}} \tag{1}$$

where q is the electronic charge, I_o is the reverse saturation current and it is a part of the reverse current in the junction caused by diffusion of minority carriers from the neutral regions to the depletion region [27], R_s is the series resistance, R_{sh} is the shunt resistance, *n* is the diode ideality factor, k is the Boltzmann's constant and T is the absolute temperature. Fig. 3 shows semi-logarithmic plot of the dark forward current of n-$ZnIn_2Se_4$/p-Si heterojunction against voltage at different temperatures. The forward current increases linearly with the increases in voltage in the range of (V < 0.7 **V**). After this range of voltage, (I-V) characteristics curves deviate from linearity. This may be attributed to the series resistance and interfacial states [28]. The value of series resistance (R_s) for n-$ZnIn_2Se_4$/p-Si heterojunction can be calculated using the relation: $\Delta V = IR_s$ [29]. As seen from Fig. 4, for a given I, the horizontal displacement between the actual curve and the extrapolated linear part of it gives the voltage drop, ΔV. The inset of Fig. 4 shows the plot of ΔV against I which gives a straight line. The value R_s was calculated from the slope of this line and it was found to be ≈ 19 kΩ at room temperature (308 K). In addition to, the junction resistance (R_j) can be determined from the (I-V) curves, where $R_j = \frac{\delta V}{\delta I}$ [30]. Fig. 5 shows the plot of R_j against voltage. At high forward bias, the junction resistance approaches a constant value that gives the value of R_s = 20 kΩ which is in a good consistent with that value calculated from Fig. 4. While at high

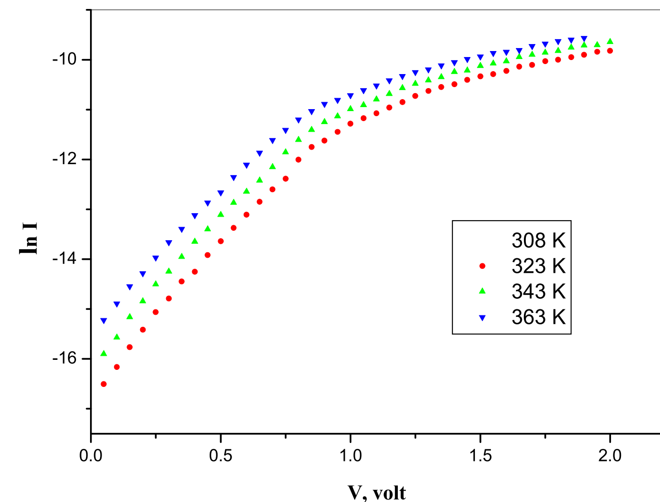

Fig. 3. Semilogarithmic plot of the forward current of n-$ZnIn_2Se_4$/p-Si heterojunction against voltage at different temperature.

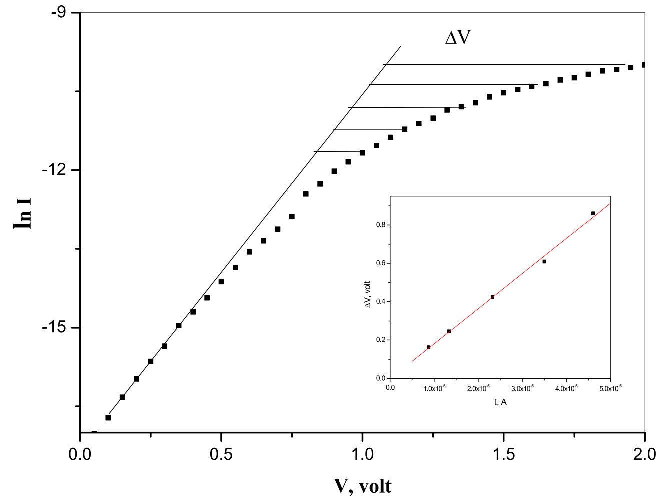

Fig. 4. Variation of lnI versus V at room temperature in forward bias. The inset shows plot of ΔV against I.

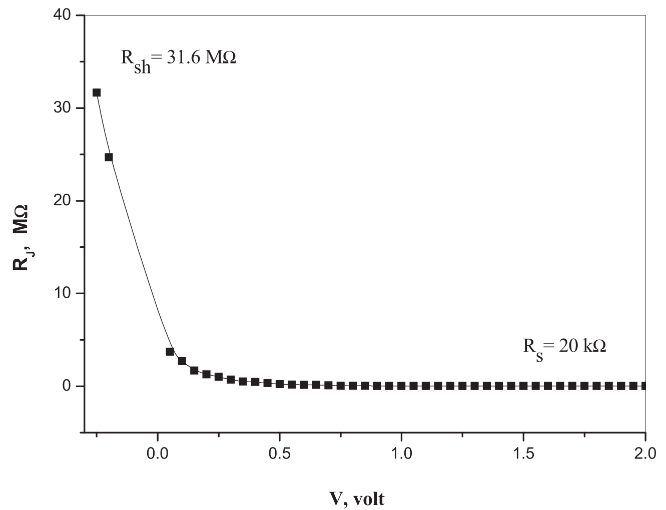

Fig. 5. Plot of R_j against voltage.

reverse bias, the junction resistance is also constant and is the value of shunt resistance. R_{sh} was found to be 31.6 MΩ at room temperature. The values of R_s and R_{sh} of n-$ZnIn_2Se_4$/p-Si heterojunction at different temperatures were calculated in the same manner at room temperature and tabulated in Table 1. The values of R_s and R_{sh} decrease as the temperature of the hetrojunction increases; this may be referred to increases in the concentration of the free carriers at high temperatures.

Moreover, the I-V curves in Fig. 3 were divided into two regions of voltages. The first region is at low forward bias (0 ≤ V ≤ 0.5 **V**), and the second region at higher forward bias (V ≥ 0.7 **V**). This behavior suggests the existence of two different mechanisms that were being responsible for the current transport mechanism in the n-$ZnIn_2Se_4$/p-Si heterojunction. At low bias voltage region, the current increases linearly with increasing applied voltage. The diode ideality factor, describes the deviation of the diode characteristics from those of the ideal diode [31], can be determined from the slope of the forward bias ln I versus voltage plot, see Fig. 3. Table 1 shows that *n* values decrease as the temperature increase from 308 K to 363 K. This result indicates that thermionic emission conduction is the predominant conduction mechanism [32] in this

region of voltage. This behavior is consistent with that obtained for p-$ZnIn_2Se_4$/n-Si by Dhruv et al. [33]. According to thermionic emission mechanism, the saturation current satisfies the following equation [34,35]:

$$I_o = AA^*T^2e^{\left(-\frac{q\varphi}{kT}\right)} \tag{2}$$

where φ is the barrier height, A is the junction area (30 mm^2) and A^* is the effective Richardson constant (32 × 10^4 $Am^{-2}K^{-2}$). The saturation current of n-$ZnIn_2Se_4$/p-Si heterojunction was obtained from the extrapolation of the forward-bias current to the lnI axis at zero voltage. The barrier height (φ) was equalized the difference in the work functions of the two materials of p-n junction [36]. The value of the barrier height was obtained by drawing a relation between ln (I_o/T^2) against (1000/T) that gives a straight line as seen in Fig. 6. Using the slope of this line, φ was calculated to be 0.3 eV.

At higher voltages ($V \geq 0.7$ **V**) the current showed dependence on the applied voltage according to the power law $I \propto V^m$, as observed in Fig. 7, where m = 2. This result indicates that the predominant operating mechanism for the current transport is space charge limited current (SCLC) with a single trap level [37]. For this region, the forward current density J can be given by Child's law [38,39] as:

$$J = \frac{9}{8}\varepsilon_z\mu\theta\left(\frac{V^2}{d^3}\right) \tag{3}$$

where ε_z is the permittivity of $ZnIn_2Se_4$ film, μ is the electron mobility, d is the thickness of $ZnIn_2Se_4$ film, and θ is the trapping factor which defined as the ratio of free to trapped charge carrier density and given by the following relation [40]:

$$\theta = \frac{N_V}{N_t}e^{\left(\frac{-E_t}{kT}\right)} \tag{4}$$

N_V is the effective density of states at the valence band edge, N_t is the total trap concentration at energy level E_t above the valence band edge. Fig. 8 shows the plot of lnI against 1000/T at V = 1 **V**. The relation is a straight line whose slope used to determine the value of trap level E_t, the calculated value of E_t was 0.23 eV.

The reverse current (I_R) of n-$ZnIn_2Se_4$/p-Si heterojunction is illustrated as a function of temperature in Fig. 9. The I_R increases with increase in temperature, indicating that this behavior is a

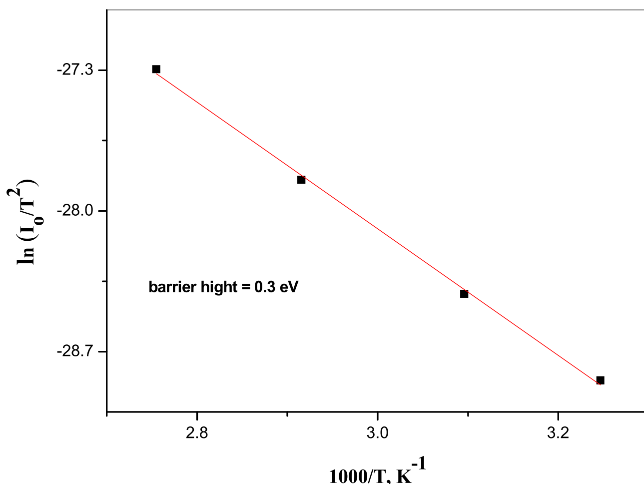

Fig. 6. Variation of ln (I_o/T^2) against (1000/T) of n-$ZnIn_2Se_4$/p-Si heterojunction.

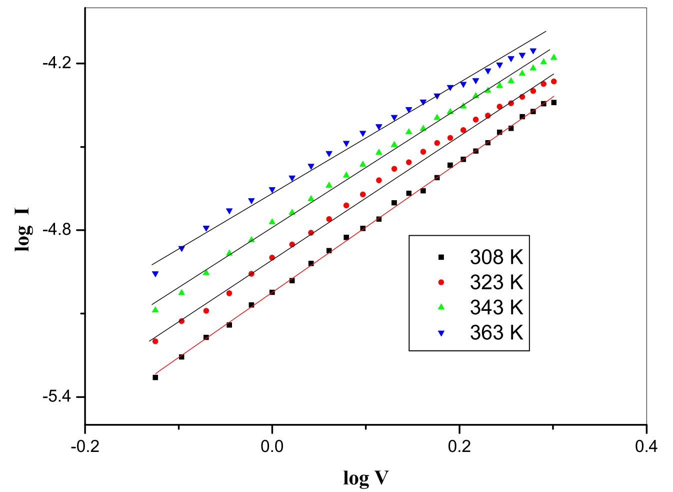

Fig. 7. Plot of logI-logV of the forward current at high voltage region of n-$ZnIn_2Se_4$/p-Si heterojunction at different temperature.

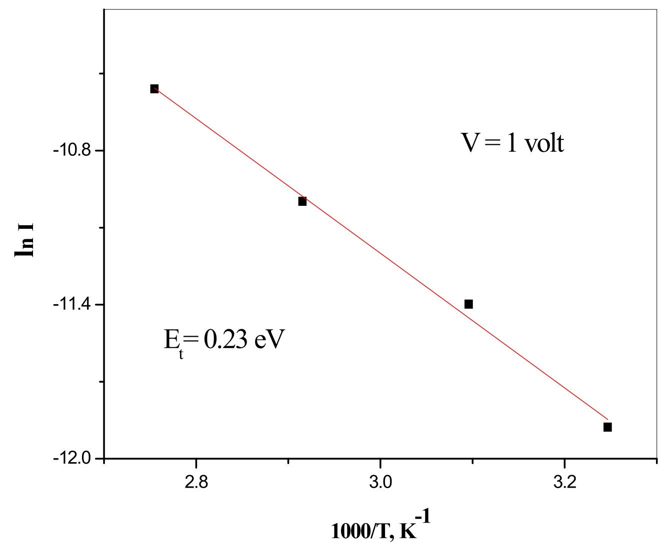

Fig. 8. Plot of lnI for the forward current in SCLC against 1000/T for n-$ZnIn_2Se_4$/p-Si heterojunction.

thermally activated process [41] and the reverse current can be expressed by the following equation [42]:

$$I_R = I_{oR}e^{\left(-\frac{\Delta E}{kT}\right)} \tag{5}$$

where I_{oR} is a constant and ΔE is the thermal activation energy. The value of ΔE is estimated from the slope of the straight line in Fig. 9 and it was found to be 0.47 eV. This value is nearly one half the value of the energy gap (1.1 eV [43]) of Si, confirming that the reverse current is due to the generation through Si rather than the $ZnIn_2Se_4$ film. This suggests that the reverse current originates in Si substrate and is controlled by generation and recombination process of the carriers in the Si bulk rather than at the $ZnIn_2Se_4$/Si interface or in the $ZnIn_2Se_4$ film itself [44].

The characteristic of capacitance – voltage measurements for a heterojunction is one of the most important tools since it determines different parameters such as built-in potential, junction capacitance, width of the depletion region and junction type [45].

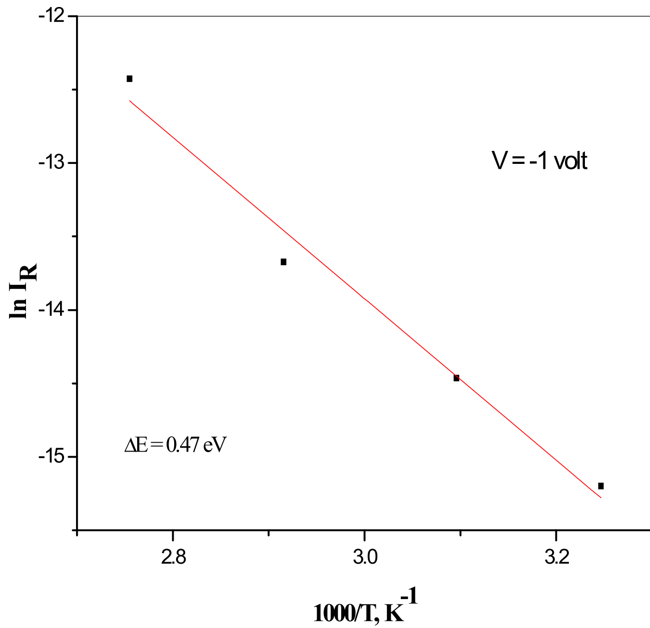

Fig. 9. Semilogarithmic plot of I_R versus 1000/T for n-$ZnIn_2Se_4$/p-Si heterojunction.

The dependence of capacitance on voltage was given by:

$$\frac{1}{C^2} = \frac{2(V_b - V)}{qA^2\varepsilon\varepsilon_o N} \tag{6}$$

where ε is the dielectric constant of p-Si, ε_o is the free space permittivity, V_b is the built-in potential at zero bias and N is the doping carrier concentration. Fig. 10 shows the plot of $1/C^2$ against voltage for Au/n-$ZnIn_2Se_4$/p-Si/Al heterojunction at room temperature at 1 MHz. This high frequency is sufficient to prevent interface states charges to contribute to the capacitance measurement [46]. As seen, ($1/C^2$ −V) variation is a linear relation in the applied voltage range, where $1/C^2$ increases linearly with increasing reverse bias indicating that the junction has an abrupt nature. That means the carrier concentration will be constant at the depletion layer [45]. The built-in voltage was calculated by extrapolating the ($1/C^2$-V) curve to the V axis as shown Fig. 10. The value of carrier concentration was calculated from the straight-line slope in Fig. 10. The values of V_b and N of n-$ZnIn_2Se_4$/p-Si heterojunction were estimated as 0.182 **V** and 2.26×10^{18} m^{-3} respectively. The capacitance of the device at zero bias (C_o) was determined and it was 0.337 nF. The width of the depletion region (W) relates the C_o by the relation [46]:

$$W = \frac{\varepsilon\varepsilon_o A}{C_o} \tag{7}$$

The calculated value of W was found to be 9.29 μm. The barrier height exists at the interface between n-$ZnIn_2Se_4$and the p-Si can be also calculated in terms of the built-in voltages from the well-known relationship [47,48]:

$$\varphi = V_b + V_P \tag{8}$$

where V_p is the potential difference between the top of the valence band in the neutral region of p-Si and the Fermi level. The value of V_p has been calculated as 0.228 eV [49,50]. According to Eq. (8), the calculated value of φ was 0.41 eV, which is more than the calculated one from (I-V) data. This result may be due to the inhomogeneity of the barrier height [47,49], contamination in the interface and deep impurity levels [33].

Fig. 11 shows a schematic presentation for energy band-diagram of $ZnIn_2Se_4$ and Si semiconductors, which formed n-$ZnIn_2Se_4$/p-Si heterojunction at thermal equilibrium. Thus, when two semiconductors with different electron affinities, band gaps and work functions are brought together to form a heterojunction diode, discontinuities form in the energy bands, thought to be due to the Fermi level alignment [32].

The current-voltage (I-V) characteristics of Au/n-$ZnIn_2Se_4$/p-Si/Al heterojunction solar cell in dark and under illumination of tungsten incandescent light bulb of 40 mW/cm^2 with active area of 0.3 cm^2 at room temperature are shown in Fig. 12. The cell parameters, the short-circuit current I_{sc}, the open-circuit voltage V_{oc} and the fill factor FF were determined from the characterization illustrated in Fig. 13 and found to be 5.98×10^{-5} mA, 0.1 V and 0.3, respectively. The value of the fill factor which was obtained in the present work in comparison with that values of other different heterojunction based on $ZnIn_2Se_4$ are shown in Table 2. The fill

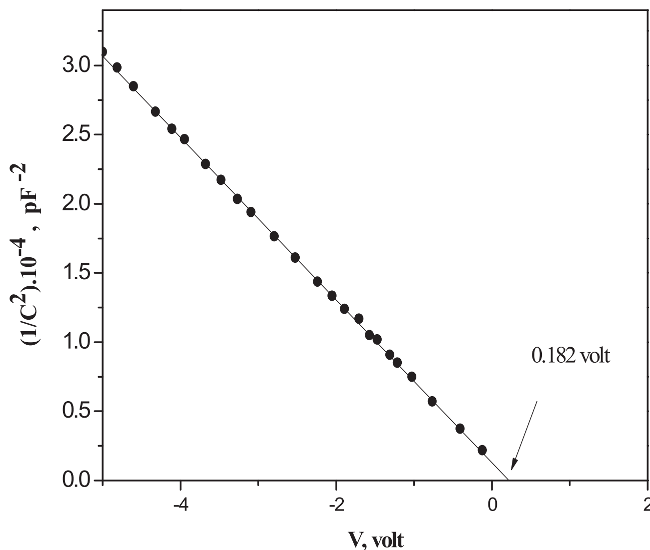

Fig. 10. Plot of $1/C^2$ against voltage of n-$ZnIn_2Se_4$/p-Si heterojunction at room temperature.

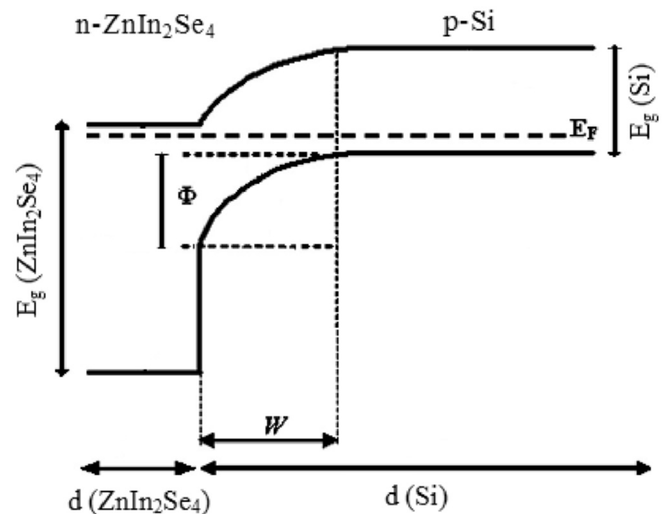

Fig. 11. Schematic of the energy band diagram of n-$ZnIn_2Se_4$/p-Si heterojunction at thermal equilibrium.

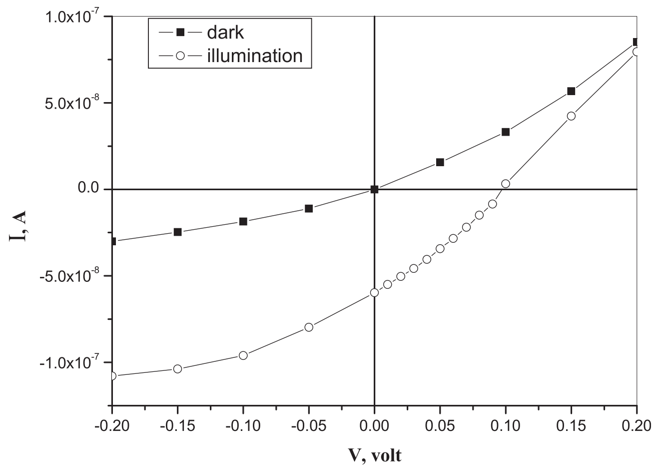

Fig. 12. I-V characteristics of Au/n-$ZnIn_2Se_4$/p-Si/Al heterojunction in dark and under illumination at room temperature.

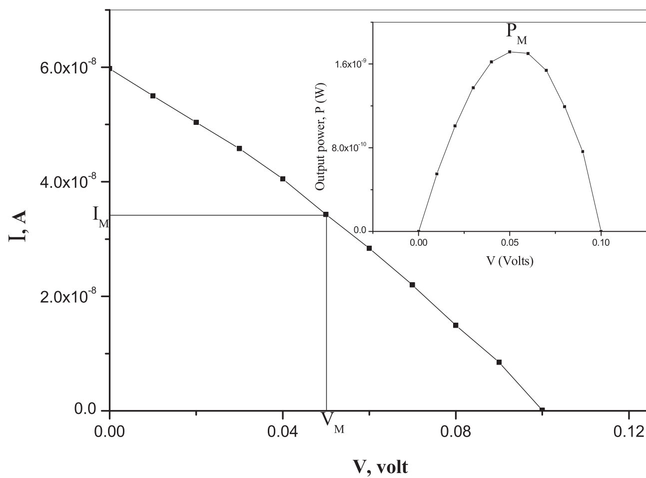

Fig. 13. I-V characterization of the cell under illumination at room temperature; the inset figure represents the variation of the output power versus voltage.

Table 2
Fill factor values for different heterojunction compared with the value obtained in the present work.

n-$ZnIn_2Se_4$/p-Si [Present work]	n-$ZnIn_2Se_4$/ polysulphide [22]	p-$ZnIn_2Se_4$/n-Si [33]
0.30	0.435	0.61

factor FF is defined as: $FF = I_M V_M / I_{sc} V_{oc}$, where I_M and V_M are the current and potential at the maximum power point (P_M). The output power of the cell is shown in the inset of Fig. 13. The values of I_M, V_M and P_M were found to be as 3.42×10^{-5} mA, 0.05 **V** and 1.71×10^{-6} mW, respectively according to Fig. 13. The low value of the fill factor is because of the effect of the high series resistance of the $ZnIn_2Se_4$ layer. In general, solar cells have a parasitic series and parallel (shunt) resistance associated with them. These types of parasitic resistance act to reduce the fill factor and subsequently the maximum output power of the cell [51]. Fig. 14 shows the current–voltage characteristics of n-$ZnIn_2Se_4$/p-Si heterojunction solar cell at room temperature in dark and under illumination conditions using an oscilloscope. A good diode with rectification behavior can be seen for the investigated n-$ZnIn_2Se_4$/p-Si heterojunction in a dark condition as shown in Fig. 14a. Fig. 14b shows the photovoltaic effect of n-$ZnIn_2Se_4$/p-Si heterojunction. The dynamic I–V characteristics support the rectification, the photovoltaic performance and the characterization of the investigated device in dark and under illumination conditions.

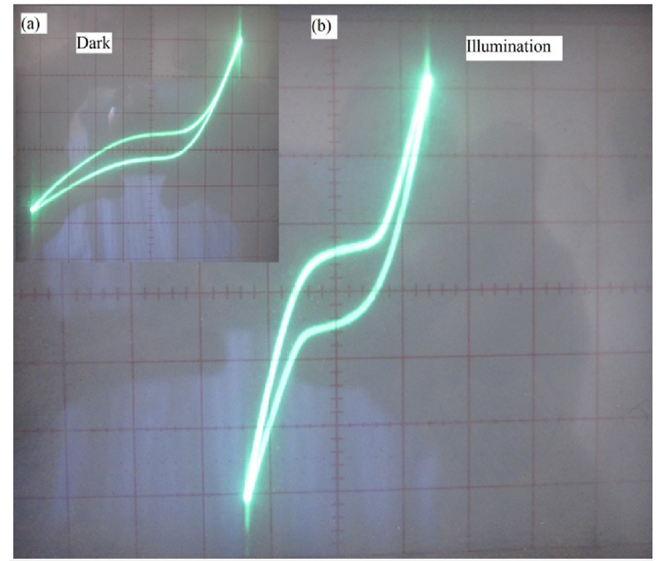

Fig. 14. Dynamic I–V characteristics (a) in dark and (b) under illumination conditions.

4. Conclusion

Noticeable progress has made in the development of high-efficiency solar cells. The components of the solar cell structure require more investigation to improve the performance. Several Zn-based chalcopyrite compounds can be used as buffer materials to reduce the optical losses and for a better band alignment in substrate of solar cells. In the present work, the electrical properties of heterojunction based on $ZnIn_2Se_4$ were investigated at different temperatures. n-$ZnIn_2Se_4$/p-Si heterojunction was fabricated using thermal evaporation technique. The device showed rectification behavior with a rectification ratio of 26.74 at room temperature. The values of R_s and R_{sh} were 20 kΩ and 31.6 MΩ, respectively at room temperature. Values of R_s and R_{sh} decrease as increasing the temperature of the heterojunction. Analysis of the I–V curves in the forward bias voltage suggests that the thermionic emission is the dominant mechanism at low voltages. At high voltages, the single-trap space charge limited current mechanism is the dominant one. The calculated barrier height of n-$ZnIn_2Se_4$/p-Si heterojunction was 0.3 eV. Under the reverse bias, the reverse current was a thermally activated process with an activation energy of 0.47 eV and the current transport mechanism was controlled by generation and recombination of carriers in p-Si. The dependence of $1/C^2$ on voltage is found to be linear indicating the abrupt nature for the heterojnuction. The built-in voltage and carriers concentrations were determined as 0.182 **V** and 2.26×10^{18} m^{-3}, respectively. The fabricated device exhibited a photovoltaic behavior and the cell parameters were estimated at room temperature and under illumination of 40 mW/cm^2.

References

[1] J. Zajic, F. Kosek, Z. Cimpl, F. Schauer, L. Stourac, J. Non Cryst. Solids 128 (1991) 1.
[2] M. Taguchi, E. Maruyama, M. Tanaka, Jpn. J. Appl. Phys. 47 (2008) 814.
[3] W.R. Fahmer, Amorphous Silicon/crystalline Silicon Heterojunnctions Solar

Cells, Springer Briefs in Applied Sciences and Technology, 2013. Chemical Industry Press, Beijing and Springer-VerlagBerling Heidelberg.
[4] J. Sritharathikhun, H. Yamamoto, S. Miyajima, A. Yamada, M. Konagai, Jpn. J. Appl. Phys. 47 (11) (2008) 8452.
[5] R.N. Gayen, S.R. Bhattacharyya, J. Phys. D. Appl. Phys. 49 (2016) 115102.
[6] Y.G. Fedorenko, M.A. Hughes, J.L. Colaux, C. Jeynes, R.M. Gwilliam, K.P. Homewood, J. Yao, D.W. Hewak, T.-H. Lee, S.R. Elliott, B. Gholipour, R.J. Curry, in: Proc. of SPIE 8982, 2014, p. 898213.
[7] P.A. Chate, D.J. Sathe, P.P. Hankare, J. Mater. Sci. Mater. Electron 22 (2) (2011) 111.
[8] I.B. Assaker, M. Gannouni, A. Lamouchi, R. Chtourou, Superlattices Microstruct. 75 (2014) 159.
[9] S. Mishra, B. Ganguli, Mater. Chem. Phys. 173 (2016) 429.
[10] L. Gastaldi, M.G. Simeone, S. Viticoli, J. Sol. Stat. Chem. 66 (1987) 251.
[11] X. Wu, T. Luo, J. Appl. Phys. 115 (2014) 014901.
[12] S. Ozaki, K.I. Muto, H. Nagata, S. Adachi, J. Appl. Phys. 97 (2005) 043507.
[13] D.K. Dhruv, A. Nowicki, B.H. Patel, V.D. Dhamecha, Surf. Eng. 31 (2015) 556.
[14] H.M. Zeyada, M.S. Aziz, A.S. Behairy, Phys. B 404 (2009) 3957.
[15] D.K. Dhruv, B.H. Patel, Mater. Sci. Semicond. Process. 54 (2016) 29.
[16] G. Alagumuthu, T. Anantha kumar, Int. J. Innov. Res. Sci. Eng. Technol. 5 (1) (2016) 178.
[17] E. Fortin, F. Raga, Solid State Commun. 14 (1974) 847.
[18] A.H. Reshak, K. Nouneh, I.V. Kityk, Jiri Bila, S. Auluck, H. Kamarudin, Z. Sekkat, Int. J. Electrochem. Sci. 9 (2014) 955.
[19] S. Mishra, B. Ganguli, Solid State Commun. 151 (2011) 523.
[20] Kai-Ning Ding, Yu-Lu Li, Yong-Fan Zhang, Chin. J. Struct. Chem. 33 (4) (2014) 519.
[21] M.M. El-Nahass, A.A. Attia, G.F. Salem, H.A.M. Ali, M.I. Ismail, Phys. B 425 (2013) 23.
[22] S.P. Yadav, P.S. Shinde, K.Y. Rajpure, C.H. Bhosale, Sol. Energy Mater. Sol. Cells 92 (2008) 453.
[23] M.M. El-Nahass, A.M. Farid, A.A.M. Farag, H.A.M. Ali, Vacuum 81 (2006) 8.
[24] A. Ashery, A.A.M. Farag, Mostafa Zeama, Superlattices Microstruct. 66 (2014) 136.
[25] H.M. Zeyada, M.M. El-Nahass, E.M. El-Menyawy, A.S. El-Sawa, Synt. Met. 207 (2015) 46.
[26] M.M. El-Nahass, H.M. Zeyada, K.F. Abd-El-rahman, A.A.A. Darwish, Sol. Energy Mater. Sol. cells 91 (2007) 1120.
[27] R.C. Dorf, Electronics, Power Electronics, Optoelectronics, Microwaves, Electromagnetics and Radar, Taylor & Francis CRC, 2006.
[28] M. Soylu, A.A. Al-Ghamdi, Omar A. Al-Hartomy, Farid El-Tantawy, F. Yakuphanoglu, Phys. E 64 (2014) 240.
[29] S. Darwish, Egypt. J. Sol. 26 (2003) 55.
[30] M.M. El-Nahass, A.M.A. El-Barry, Ind. J. Pure Appl. Phys. 45 (2007) 465.
[31] H.M. Zeyada, M.M. El-Nahass, E.M. El-Menyawy, A.S. El-Sawah, Synth. Met. 207 (2015) 46.
[32] E.M. Nasir, Inter. J. Eng. Adv. Technol. 3 (2013) 425.
[33] D.K. Dhruv, B.H. Patel, D. Lakshminarayana, Mater. Res. Innov. 20 (4) (2016) 285.
[34] H.M. Zeyada, M.M. Makhlouf, M.M. El-Shabaan, M.H. Zeyada, Microelectron. Eng. 157 (2016) 35.
[35] D.A. Neamen, Semiconductor Physics and Devices, Richard D. Irwin, Inc., USA, 1999.
[36] H.S. Nalwa, Handbook of Surfaces and Interfaces of Materials, Acadimic press, London, Uk, 2001, p. 465.
[37] M.S. Roy, P. Balraju, Y.S. Deol, R.K. Mishra, V.S. Choudhary, G.D. Sharma, Sol. Energy Mater. Sol. Cells 92 (2008) 1516.
[38] K.C. Kao, W. Hwang, Electrical transport in solids, with particular reference to organic semiconductors, in: first ed.International Series in the Science of the Solid State, vol. 14, Pergamon Press, Oxford, 1981.
[39] K.H.S. Karimov, I. Qazi, S.A. Moiz, I. Murtaza, Optoelectron. Adv. Mater. Rapid Commun. 2 (4) (2008) 219.
[40] K.R. Rajesh, C.S. Menon, Ind. J. Pure. Appl. Phys. 43 (2005) 964.
[41] M.M. Ahmed, Kh S. Karimov, S.A. Moiz, IEEE Trans. Electron. Dev. 51 (2004) 495.
[42] M.M. EL-Nahass, A.M. Farid, H.H. Amer, K.F. Abdel-Rrahman, H.A.M. Ali, Mater. Sci. Pol. 27 (2) (2009) 385.
[43] V. Rajendran, A. Marinani, Materials Science, Tata McGraw-Hill, New Delhi, 2004.
[44] R. Ao, L. Kilmmert, D. Haarer, Adv. Mater. 7 (1995) 495.
[45] H.A. Hadi, I.H. Hashim, J. Electron Devices 20 (2014) 1701.
[46] M.H. Ali, Curr. Sci. Int. 4 (1) (2015) 1.
[47] M.M. El-Nahass, H.S. Metwally, H.E.A. El-Sayed, A.M. Hassanien, Synth. Met. 161 (2011) 2253.
[48] A.A. Hendi, E.F.M. El-Zaidia, Synt. Met. 161 (2011) 2253.
[49] N. Kavasoglu, C. Tozlu, O. Pakma, A.S. Kavasoglu, S. Ozden, B. Metin, O. Birgi, S. Oktik, Synth. Met. 159 (2009) 1880.
[50] A.S. Riad, Thin Solid Films 370 (2000) 253.
[51] G.M. Masters, Renewable and Efficient Electric Power Systems, Wiley, Hoboken, 2004.